J. Fluid Mech. (1999), *vol.* 397, *pp.* 73–98. Printed in the United Kingdom

Flow between time-periodically co-rotating cylinders

By PATRICIA ERN† AND JOSÉ EDUARDO WESFREID
Laboratoire de Physique et Mécanique des Milieux Hétérogènes, UMR CNRS 7636,
Ecole Supérieure de Physique et Chimie Industrielles de Paris – ESPCI,
10, rue Vauquelin, 75231 Paris cedex 05, France

(Received 28 October 1998 and in revised form 16 May 1999)

We consider oscillatory flows between concentric co-rotating cylinders at angular velocity $\Omega(t) = \Omega_m + \Omega_o \cos \omega t$ as a prototype to investigate the competing effects of centrifugal and Coriolis forces on the flow stability. We first study by flow visualization the effect of the mean rotation Ω_m on the centrifugal destabilization due to the temporal modulation. We show that increasing the mean rotation first destabilizes and then restabilizes the flow. The instability of the purely azimuthal basic flow is then analysed by investigating the dynamics of the axial velocity component of the vortex structures. Velocity measurements performed in the rotating frame of the cylinders using ultrasound Doppler velocimetry show that secondary flow appears and disappears several times during a flow period. Based on a finite-gap expression for the basic flow, linear stability analysis is performed with a quasi-steady approach, providing the times of appearance and disappearance of secondary flow in a cycle as well as the effect on the instability threshold of the mean rotation. The theoretical and numerical results are in agreement with experimental results up to intermediate values of the frequency. Notably, the flow periodically undergoes restabilization at particular time intervals.

1. Introduction

Interest in time-periodic flows has been stimulated both by the presence of oscillatory flows in many natural systems (like blood flow in arteries or sediment transport in estuaries) and as a first approach to analyse noise effects on nonlinear systems with the introduction of a temporal modulation on a flow control parameter. Motivation for the latter was sparked by the success of studies concerning well-characterized instabilities such as Taylor–Couette or Rayleigh–Bénard configurations. Growing fascination was then fuelled by the almost simultaneous appearance of contradictory results suggesting either a destabilizing or stabilizing effect of the superimposed temporal modulation on these stationary unstable flows, as well as a debate on the strength of the effect. For the Rayleigh–Bénard convection system, reviews are given by Ahlers, Hohenberg & Lücke (1985) who generalize the Lorenz model and analyse boundary conditions and system size effects and by Schmitt & Lücke (1991) who derive the nonlinear amplitude equation governing the transition. Concerning the Taylor–Couette configuration, concomitant works by Kuhlmann, Roth & Lücke (1989) and Barenghi & Jones (1989) gave a comprehensive analysis, including the effect of the temporal

---

† Present address: Institut de Mécanique des Fluides, UMR CNRS/INP-UPS 5502, Allée du Professeur Camille Soula, 31400 Toulouse, France.

modulation on the onset of instability and the nonlinear behaviour of the instability rolls.

On the other hand, for purely oscillatory flow, there is no stationary unstable flow serving as a reference to quantify the modulation effect. Because of the non-separability of space and time variables, it is difficult to treat the instability analytically and the problem has to be solved numerically. The stability of oscillatory flows is related to the development and stability of Stokes layers at the boundaries. The usual prototype of oscillatory flows is the plane Stokes layer (Davis 1976). In the present work, we are concerned with Stokes layers generated over curved walls, whose destabilization is induced by centrifugal effects (Seminara & Hall 1976, 1977; Papageorgiou 1987; Horseman, Bassom & Blennerhassett 1996). The instability then appears as spatially periodic counter-rotating vortices aligned with the main flow, like Taylor, Dean or Görtler vortices.

In this framework, it is interesting to come back to the Taylor–Couette configuration to study a flow where the destabilization is linked to the development of centrifugal Stokes layers. We consider here the stability of the flow developing when both cylinders rotate *jointly* at the same angular velocity $\Omega(t) = \Omega_m + \Omega_o \cos \omega t$ and for a range of values of the mean velocity Ω_m. Previous studies by flow visualization are those by Aouidef *et al.* (1994) for $\Omega_m = 0$ and by Tennakoon *et al.* (1997) for one value of the mean rotation Ω_m and for counter-rotating cylinders for $\Omega_m = 0$. They also analysed their systems as the instability of the Stokes layer in the plane configuration. In our study, we will consider the more realistic general case of Stokes layers including curvature effects. A first contribution of this paper is to present velocity measurements characterizing the temporal behaviour of this oscillatory flow. The instability of the purely azimuthal basic flow is analysed by investigating the dynamics of the axial velocity component of the vortex structures that appear and disappear during an oscillation cycle. Up to intermediate values of the forcing frequency, this behaviour is recovered with a quasi-steady finite-gap analysis even when mean rotation effects are included.

Our second concern in this work is with the effect of rotation on centrifugal instabilities, which is inferred here by the influence of the mean rotation term Ω_m on the centrifugal destabilization due to the periodic rotation at $\Omega_o \cos \omega t$. Interest in the problem of rotation–instability interaction stemmed from its occurrence in geophysical (Tritton & Davies 1985) and industrial flows (such as Görtler flow around rotating blades in turbines, see for instance Aouidef, Wesfreid & Mutabazi 1992). A first step in the comprehension of these systems was given by the evidence that the Coriolis force can generate instability in a stable flow, like in Poiseuille flow (Alfredsson & Persson 1989). Further advances showed that rotation might modify turbulence (Bidokhti & Tritton 1992; Cambon *et al.* 1994) or instability, having either a stabilizing or destabilizing effect. For instance, destabilization may be observed in the development of three-dimensional perturbations when rotation and flow vorticity vectors are parallel or anti-parallel, like in mixing layers or in boundary layer flows. Other works have addressed the effect of rotation on Rayleigh–Bénard convection (Chandrasekhar 1981) or on a Taylor–Couette flow with the rotation axis perpendicular to the cylinder axis (Wiener *et al.* 1990; Ning *et al.* 1991). Studies concerned specifically with the competing effects of Coriolis and centrifugal forces on flow stability have been reported for rotating Dean flow (Matsson & Alfredsson 1990, 1994) or rotating Görtler flow (Zebib & Bottaro 1993; Pexieder 1996) showing that depending on its direction, the Coriolis force may inhibit or enhance the centrifugal destabilization. In this paper, we investigate the effect of rotation on centrifugal Stokes layers. Moreover, in our experimental setup, thanks to its reduced size compared to a water channel in a rotating platform, this effect is explored over a large range of flow parameters.

The procedure adopted in the paper is the following. In § 2, we present the basic flow expression for a finite gap between the cylinders as well as the parameters of the system. Section 3 is devoted to the experimental setup and techniques. Flow visualization results showing the effect of the mean rotation on flow stability are addressed in § 4. Section 5 presents ultrasound Doppler velocimetry results concerning the time behaviour of the vortex structure. Section 6 investigates the flow instability by means of a theoretical and numerical analysis.

2. Preliminaries

In this section, we present the basic flow of our configuration and define the control parameters of our system. We consider two concentric infinitely long cylinders of radii R_1 and $R_2 = R_1 + d$ rotating at the angular velocities

$$\Omega_{m1} + \Omega_{o1} \cos \omega t \quad \text{for} \quad x = 0 \quad \text{and} \quad \Omega_{m2} + \Omega_{o2} \cos \omega t \quad \text{for} \quad x = 1,$$

where x stands for the dimensionless radial coordinate defined by $r = R_1 + xd$. Our aim is to obtain the finite-gap expression in cylindrical coordinates (r, θ, z) for the purely azimuthal basic flow $V_B(x,t)$.

Using the viscous diffusion time scale corresponding to Stokes layer formation $\tau_v = d^2/\nu$, where ν is the kinematic viscosity, we define the non-dimensional frequency of modulation

$$\sigma = \frac{\omega d^2}{\nu}.$$

It is also convenient to introduce the frequency parameter γ, scaling the Stokes layer thickness $\nu/(\omega d)$ to the half-gap size $d/2$,

$$\gamma = \sqrt{\frac{\omega d^2}{2\nu}} = \sqrt{\frac{\sigma}{2}}.$$

We define the associated complex frequency $\gamma_c = \gamma(1 + \mathrm{i})$ and the non-dimensional gap $\delta = d/R_1$. We denote $\mu = \delta^{-1}$, $\Gamma_m = \Omega_{m2}/\Omega_{m1}$, $\Gamma_o = \Omega_{o2}/\Omega_{o1}$ and $\hat{Ro} = \Omega_{m1}/\Omega_{o1}$. The basic flow V_B, scaled by $R_1\Omega_{o1}$, is given in the laboratory frame by

$$V_B(x,t) = V_m(x) + \mathrm{Re}\,(V_s(x)\exp{(\mathrm{i}\sigma\tau)}), \tag{2.1}$$

with $\tau = t/\tau_v = t\nu/d^2$ and where the mean flow component V_m is given by

$$V_m(x) = \frac{(\Gamma_m(1+\delta)^2 - 1)(1 + x\delta)^2 + (1 - \Gamma_m)(1+\delta)^2}{((1+\delta)^2 - 1)(1 + x\delta)}\,\hat{Ro}. \tag{2.2}$$

The complex velocity V_s has been reported in Tustaniwskyj & Carmi (1981) and Ern (1998). Using the asymptotic expansion of the product of Bessel functions appearing in V_s, Ern (1998) has derived a simpler analytical expression for V_s. At the first order in the gap δ, the complex velocity V_s reads

$$V_s(x) = \frac{\sinh{(\gamma_c(1-x))} + \Gamma_o\,(1+\delta)^{3/2}\sinh{(\gamma_c x)}}{(1+x\delta)^{1/2}\sinh{(\gamma_c)}}. \tag{2.3}$$

For convenience one writes $V_s = V_1 - \mathrm{i}V_2$ so that the basic flow V_B can be written

$$V_B(x,t) = V_m(x) + V_1(x)\cos\sigma\tau + V_2(x)\sin\sigma\tau, \tag{2.4}$$

with the following expressions for V_1 and V_2:

$$V_1(x) = \frac{(A(x) + \Gamma_o\,(1+\delta)^{3/2}C(x))\sinh\gamma\cos\gamma + (B(x) + \Gamma_o(1+\delta)^{3/2}D(x))\cosh\gamma\sin\gamma}{(1+x\delta)^{1/2}(\cosh^2\gamma - \cos^2\gamma)}, \tag{2.5}$$

$$V_2(x) = \frac{(A(x) + \Gamma_o\,(1+\delta)^{3/2}C(x))\cosh\gamma\sin\gamma - (B(x) + \Gamma_o(1+\delta)^{3/2}D(x))\sinh\gamma\cos\gamma}{(1+x\delta)^{1/2}(\cosh^2\gamma - \cos^2\gamma)}, \tag{2.6}$$

where

$$A(x) = \sinh(\gamma(1-x))\cos(\gamma(1-x)), \quad B(x) = \cosh(\gamma(1-x))\sin(\gamma(1-x)),$$

$$C(x) = \sinh(\gamma x)\cos(\gamma x) \quad \text{and} \quad D(x) = \cosh(\gamma x)\sin(\gamma x).$$

Expressions (2.5)–(2.6), valid at the first order in δ, will be termed the finite-gap approximation. An estimate of the validity of this approximation is obtained when the second-order terms in δ can be neglected. Expressions (2.5)–(2.6) are valid as long as the condition (Ern 1998)

$$f(\gamma, \delta) = \delta^2\,\frac{3\sqrt{2\gamma^2 - 2\gamma + 1}}{16\gamma^2} \ll 1 \tag{2.7}$$

holds. In our experimental configuration, the gap is $\delta = 0.112$ so that we get $f(\gamma, 0.112) \leqslant 10^{-2}$ as long as $\gamma \geqslant 0.41$.

The steady outer and modulated inner cylinder case studied for example by Kuhlmann *et al.* (1989) can be recovered in (2.5)–(2.6) for $\Gamma_m = \Gamma_o = 0$, and the 180°-out-of-phase cylinder case from Tennakoon *et al.* (1997) for $\Gamma_m = 1$ and $\Gamma_o = -1$. In this paper, we focus our attention on the particular case $\Gamma_m = \Gamma_o = 1$ corresponding to co-rotating modulated cylinders, the imposed angular velocity of both cylinders being denoted $\Omega(t) = \Omega_m + \Omega_o\cos(\omega t)$. We define two non-dimensional parameters that govern the stability of our system: the Taylor number Ta proportional to the modulation amplitude Ω_o

$$Ta = \frac{\Omega_o R_1^{1/2} d^{3/2}}{\nu},$$

and the rotation number Ro, the inverse of the Rossby number, defined by

$$Ro = \delta\,\hat{R}o = \frac{d}{R_1}\frac{\Omega_m}{\Omega_o}.$$

At a given forcing frequency γ, the critical Taylor number Ta_c corresponds to the modulation amplitude Ω_o needed to produce an instability at a given uniform rotation Ω_m.

Finally, it will be useful to consider two particular cases. In the low-frequency regime $\sigma \ll 1$, the velocity momentum has time to diffuse by viscosity in the gap d during a period. A simplified basic flow expression can then be obtained by the method of Eagles (1977), as shown by Ern (1997). We get

$$V_B = (\hat{R}o + \cos\sigma\tau)(1 + \delta x) + \tfrac{1}{2}\sigma x(1-x)(1 + \tfrac{1}{2}\delta)\sin\sigma\tau + o(\sigma\delta). \tag{2.8}$$

At a given time, the principal contribution is given by a solid-body rotation term in phase with the forcing. The second term is a Poiseuille parabolic profile with a phase opposite to that of the forcing.

On the other hand, at high frequencies $\gamma \gg 1$, the Stokes layer thickness is much

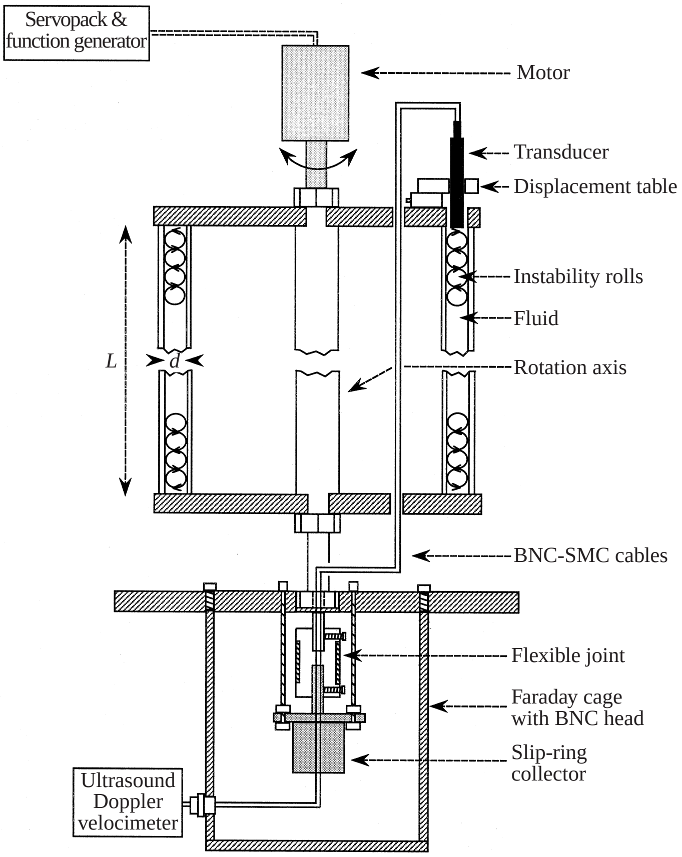

FIGURE 1. Sketch of the experimental setup with ultrasound Doppler velocimetry. (Not to scale; $L = 305\,\text{mm}$, $d = 7.75\,\text{mm}$ and inner cylinder radius $R_i = 69.25\,\text{mm}$.)

smaller than the gap size d. The basic flow V_B can then be written as

$$V_B = V_m + \frac{\mathrm{e}^{-\gamma x}}{(1+\delta x)^{1/2}} \cos(\gamma x - \sigma\tau) + (1+\delta)^{3/2} \frac{\mathrm{e}^{-\gamma(1-x)}}{(1+\delta x)^{1/2}} \cos(\gamma(1-x) - \sigma\tau) \qquad (2.9)$$

and is the sum of two velocity profiles of Stokes layer type, with an amplitude damped (amplified) spatially for the inner (outer) cylinder with respect to the plane configuration.

3. Experimental setup

3.1. *Apparatus*

The experimental configuration is presented in figure 1. It consists of a Taylor–Couette cell of two concentric cylinders with gap $d = 7.75\,\text{mm}$ containing the fluid. The cylinders are closed by a top and bottom plate that rotate with the cylinders. The height of the cylinders is $L = 305\,\text{mm}$ so that the aspect ratio of the cell is $L/d = 39$ and the central core of the fluid can be considered to be unaffected by end effects. The inner cylinder of external radius $R_i = 69.25\,\text{mm}$ is made from black-anodized Dural in order to facilitate flow visualization. The external cylinder is made from Plexiglas, with internal radius $R_o = 77 \pm 0.1$ mm. The non-dimensional gap is $\delta = 0.112$ and the radii of the cylinders have ratio 0.899.

The cylinders rotate jointly via a brushless servomotor Yaskawa USAREM 01-CE2K +MRC 300-1/20. A time-periodic signal is imposed on the motor by a Hewlett Packard 33120A-15MHz function generator connected to a servopack CACR-SR01AC. Using the back signal from the motor tachometer to the servopack, we have checked that the effective rotation of the motor and the cylinders corresponds to the signal imposed by the function generator.

3.2. *Flow detection techniques*

3.2.1. *Flow visualization*

Flow visualization is performed using a de-ionized water solution with 2% Kalliroscope rheoscopic concentrate AQ-1000 and 1% SQ-1000 bacterial stabilizer. Kalliroscope flakes are a classical visualization tool for Taylor–Couette flows (Andereck, Liu & Swinney 1986), because of their properties of reflection and their tendency to align along streamlines (Gauthier, Gondret & Rabaud 1998). At a given frequency γ and mean rotation Ω_m, the determination of the onset of instability is performed by increasing the modulation amplitude Ω_o by steps of 2.632×10^{-2} rad s^{-1} corresponding to a change in Taylor number of about 5 units. We wait for a sufficient period of time for the flow to adapt to each new configuration. For instance, for $\gamma = 1$, we wait for ten cycles T (about 15 min). As $T = (\pi/\gamma^2)\tau_v$ where $\tau_v = d^2/\nu$ is the viscous diffusion time, this interval is larger than 30 τ_v. We then examine the flow during five, or more, cycles to detect the instability.

By visualization, the instability appears as transient shadowed black and white streaks. As the amplitude Ω_o of the forcing is increased, the instability appears more clearly as pulsed Taylor–Couette rolls. We assume that in this system no long-term development of the instability is to be expected since the flow undergoes periodic restabilization when the cylinders reverse their rotation, as will be described later with the velocity measurements. For this reason, we have also chosen to increase the modulation amplitude when the forcing is decreasing in time and the flow is restabilizing. In spite of its simplicity, eye observation is a very accurate detection tool, far better than the observation obtained with a 256 grey levels CCD camera or other systems as also indicated by Walsh (1988) in his experiment with a time-periodic inner cylinder rotation. Our determination of the instability threshold has a reproductibility of 5%. Error in the Taylor number values, mainly due to the determination of the viscosity, is less than 3%.

3.2.2. *Ultrasound Doppler velocimetry*

Velocity measurements have been performed with a Signal Processing Dop 1000 ultrasound Doppler velocimeter. In our case, this technique is particularly interesting as the reduced size of the transducer allows us to perform easily measurements in the rotating frame of the cylinders. Moreover, the apparatus delivers a velocity profile quasi-instantaneously. We have measured the axial profile of the axial component of the velocity. This quantity is particularly relevant as it constitutes a direct indication of the presence of the vortex structure and allows its characterization (see for instance, Ahlers *et al.* 1986; Heinrichs *et al.* 1988; Cooper *et al.* 1985; Kuhlmann *et al.* 1989 and Takeda *et al.* 1993*b*).

As shown in figure 1, the measurements are performed in the rotating frame of the cylinders and transfered to the laboratory frame for analysis. On the top cover of the cylinders, and following their rotation, the ultrasound transducer is held vertically on a micrometric displacement table which allows radial motion of the transducer. To avoid parasite reflections the transducer is directly in contact with the fluid. The signal is transfered to a slip-ring Litton Poly-Scientific AC 4023-12 protected in a Faraday cage. The cables of the slip-ring non-rotating part are connected to a BNC head located in the Faraday cage.

The operating principle of the ultrasound Doppler velocimeter has been given by Willemetz (1990) and Takeda (1991). We used a transducer of 8 MHz emitting frequency, shifting between an emission and reception state. The pulse repetition frequency f_p was taken as small as possible ($f_p \approx 488.3$ Hz) in order to have the lowest possible velocity detection range (6 mm s^{-1}). Data for a given time results from averaging the last six profiles. The induced acoustic field is composed of a cylindrical Fresnel region of radius $r = 2.5$ mm which starts to expand conically at a distance of 3 cm from the transducer with an angle of 2.9° for the Frauenhofer principal lobe. At a given depth, the measured axial velocity is a mean over the section of this volume. Measurements are performed up to a distance of 9 cm from the transducer with an axial resolution of 0.8 mm. For data analysis, we only considered the last 50 measured spatial points, which correspond in depth to a distance from the transducer bigger than 5 cm. This avoids the inclusion of the end effects of the cylinders. Depending on the values of the parameters, 50 spatial points correspond to about 3 to 5 Taylor vortices. The working fluid is a de-ionized water solution with 30% by mass of glycerol seeded with 3 g l^{-1} of Griltex COPA 11P1 4104320/09 particles and containing 0.05% of Kalliroscope AQ-1000. Except for the mono-dispersity of the particles the same mixture was used in the Taylor–Couette experiments of Takeda, Fisher & Sakakibara (1993*a*). This mixture was found to be an appropriate ultrasound reflector which allowed simultaneous flow visualization. Our particles have a maximum size of 80 μm and a density of 1.07 g cm^{-3}. In this case, the error in the estimation of the Taylor number is lower than 3.5%. For the velocity measurements, the noise level (or background signal) is estimated to be less than 0.15 mm s^{-1} thanks to the Faraday cage isolation.

4. Coriolis force effect: results by visualization

When $\Omega_m = Ro = 0$, the basic flow has no mean component and the instability is generated by the phase lag of the flow with respect to its moving boundaries. Detailed linear stability analysis of this flow has been carried out with Floquet calculations in the small-gap approximation ($\delta \to 0$) and visualization experiments by Aouidef *et al.* (1994). Results showed that for all modulation frequencies γ, the flow is destabilized. Maximal destabilization (lower $Ta_c(\gamma)$) is achieved for intermediate frequencies $\gamma \approx 2$, whereas the flow stability increases for lower and higher frequencies. The same tendency was observed for one value of the mean rotation ($\Omega_m = 1.26$ rad s^{-1}) by Tennakoon *et al.* (1997). In this work, we are interested in the Coriolis force contribution to the flow instability. We thus study, at a given frequency, the amplitude of the temporal modulation needed to destabilize different solid-body rotation flows. We investigate the behaviour of the threshold Ta_c as a function of the rotation number Ro for different frequencies γ.

4.1. *Flow stability with mean rotation*

Figure 2 reports the evolution of the critical Taylor number Ta_c as a function of the rotation number Ro for several frequencies γ. At a given frequency, the parameter regimes above the curve correspond to an unstable flow characterized by the presence

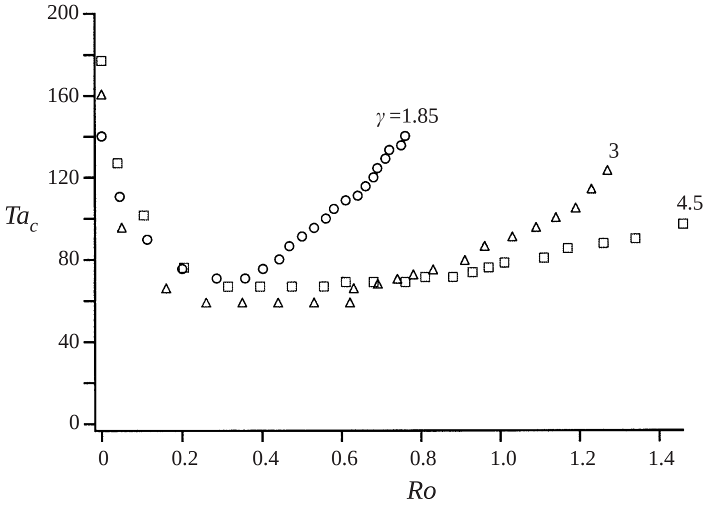

FIGURE 2. Examples of the evolution of the instability threshold Ta_c as a function of the rotation number Ro for different frequencies γ ($\delta = 0.112$).

of counter-rotating time-dependent rolls, whereas under the curve, the flow is stable, the velocity being the purely azimuthal velocity V_B.

Whatever the forcing frequency γ, we observe a maximal destabilization of the flow (lower Ta_c) for an intermediate rotation number Ro (in general between 0.3 and 0.6). When the rotation number goes to zero, we observe a rapid growth of Ta_c towards the purely centrifugal case when $Ro = 0$. For large Ro, we also observe an increasing flow stability as expected from the Taylor–Proudman constraint. For all forcing frequencies, we find a destabilizing followed by a restabilizing effect as the mean rotation is increased.

4.2. *Considerations for large rotation numbers*

At large rotation numbers Ro, one can show that the Taylor–Proudman theorem applies. Consider the non-dimensional Navier–Stokes equations in the rotating frame at the angular velocity Ω_m, for frequencies of order 1, as explored experimentally. The flow is induced by the temporal modulation so that the characteristic velocity scale is $V \sim \Omega_o R$ and the external temporal scale is $\tau \sim \omega^{-1}$. Hence, at large Ω_m and large Ro, the Ekman number $E = \nu/(\Omega_m d^2) \ll 1$ and the Rossby number $\epsilon = 1/Ro = V/(\Omega_m d) \ll 1$, so that both inertia and viscous diffusion terms are negligible in the equation. Moreover, the time-derivative prefactor is $1/(\Omega_m \tau) \sim \omega/\Omega_m \ll 1$. The equation thus reduces to the stationary Taylor–Proudman relation $2\Omega \wedge \boldsymbol{U} = \nabla P$ which equates the Coriolis term to the pressure gradient, the latter including classically the hydrostatic contribution and the centrifugal force.

We have also analysed the flow restabilization at large Ro using the Rayleigh criterion. For inviscid flows subjected to rotation, a necessary and sufficient condition for centrifugal stability is given by the generalized Rayleigh criterion (Mutabazi, Normand & Wesfreid 1992; Mutabazi & Wesfreid 1993; Kloosterziel & van Heijst 1991; Leblanc & Cambon 1997). For time-dependent flows, a sufficient condition is that the criterion is met at all t (Rosenblat 1968). The stability condition reads

$$\Phi = \left(\frac{\delta}{1+\delta x} V_{Bo} + Ro\right)\left(\frac{\partial V_{Bo}}{\partial x} + \frac{\delta}{1+\delta x} V_{Bo} + 2Ro\right) > 0,$$

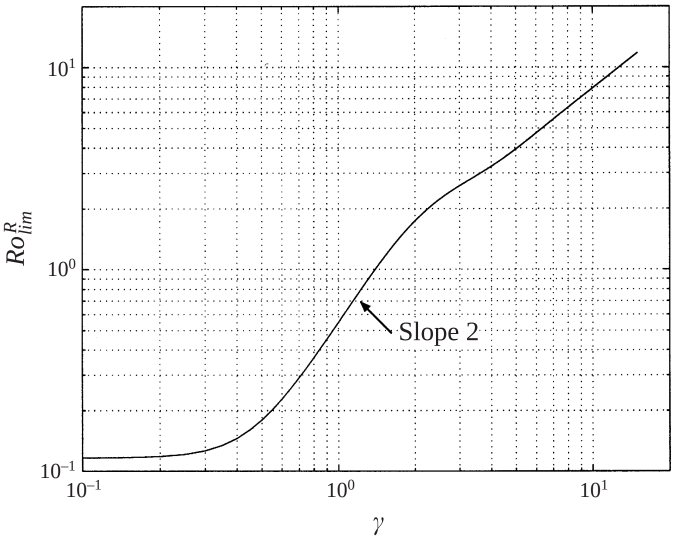

FIGURE 3. Evolution predicted by (4.1) of Ro^R_{lim} as a function of γ, on a logarithmic scale ($\delta = 0.112$). The region under the curve gives the parameter regime for which instability may be observed.

where V_{Bo} is the flow without mean rotation $V_{Bo}(x,\tau) = V_1(x)\cos(\sigma\tau) + V_2(x)\sin(\sigma\tau)$ with V_1 and V_2 given by (2.5) and (2.6), δ being the non-dimensional gap. The flow restabilization at large rotation numbers is contained in the Rayleigh criterion. Indeed, when Ro is predominant, Φ becomes positive and the flow is stable with respect to axisymmetric perturbations. More precisely, the sign of Φ is given by the absolute vorticity $\partial V_{Bo}/\partial x + \delta V_{Bo} + 2Ro$ with $\delta^2 \ll 1$. The marginal condition for centrifugal instabilities ($\Phi = 0$) thus defines, for any frequency γ, an inviscid limit rotation number Ro^R_{lim} given by

$$Ro^R_{lim}(\gamma) = \frac{1}{2}\left|\frac{\partial V_{Bo}}{\partial x}(x,\tau) + \delta V_{Bo}(x,\tau)\right|_{max}. \tag{4.1}$$

For rotation numbers larger than $Ro^R_{lim}(\gamma)$, no three-dimensional centrifugal flow can be observed. It is straightforward to show (Ern 1997) that the maximum value in x is obtained for $x = 1$. The evolution of Ro^R_{lim} with γ is presented in figure 3 on a logarithmic scale, defining the rotation number–frequency regimes for which centrifugal instability may develop. Figure 3 shows in particular a γ^2 behaviour of Ro^R_{lim} at low to order-1 frequencies. This behaviour will be also obtained by the linear stability analysis carried out in § 6.2.1.

5. Velocity measurement results

We have followed the real time evolution of the profile along the z-axis of the axial velocity component $w(z,t)$. We observe a repeated growth and decay in amplitude of a sinusoidal-shape profile, which corresponds to the counter-rotating vortices. In order to characterize the temporal behaviour of the vortex structure, we use the root-mean-square value $W_{rms}(t)$ corresponding to the variation along the z-axis of the axial velocity values. At any time, from the measured velocity profile, we extract the

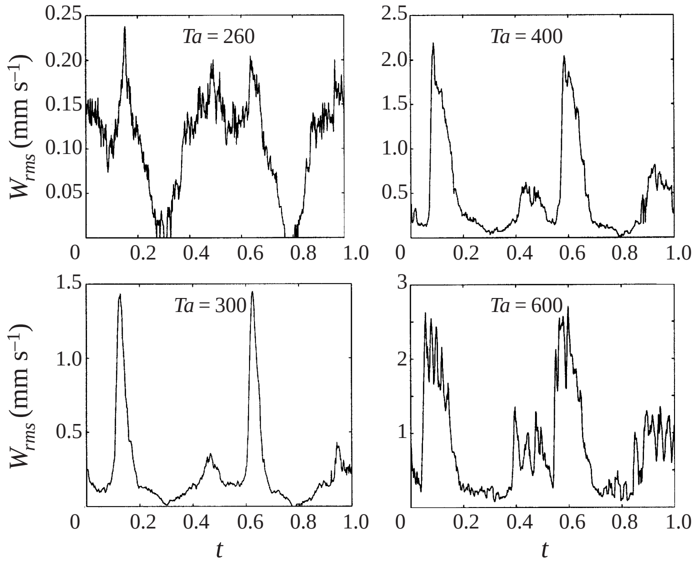

FIGURE 4. Examples of the behaviour of W_{rms} over a period for several Taylor numbers Ta and for $\gamma = 1$ and $Ro = 0$ ($\delta = 0.112$). Note the different scales used for W_{rms} in the plots. The beginning of the period corresponds to cylinders at rest.

value

$$W_{rms}(t) = \left(\frac{1}{N} \sum_{i=1}^{N} w^2(z_i, t) \right)^{1/2} \tag{5.1}$$

for $N = 50$, which provides a global description of the flow. Using the external trigger of the velocimeter, we have synchronized the data acquisition with the function generator signal. The time origin has been chosen to be $t = -\frac{1}{2}\pi$ for a forcing in $\cos t$, thus corresponding to zero velocity for the cylinders.

Figure 4 presents the behaviour of W_{rms} over a temporal period for different Taylor numbers Ta and for $\gamma = 1$ and $Ro = 0$. Typically, when $\gamma = 1$, a period corresponds to ≈ 90 s and is composed of about 1000 data points. Figure 5 presents the case $\gamma = 2$. The instability rolls are difficult to observe near onset. For instance, at $Ta = 220$ for $\gamma = 1$, thus slightly above the instability onset observed by visualization ($Ta_c = 205$), it is very difficult to distinguish the secondary flow from the background signal which is lower than $0.15\,\mathrm{mm\,s^{-1}}$. Only at larger Taylor numbers (around 300), can peaks with a large W_{rms} amplitude be observed. The peaks correspond to the successive appearance and disappearance of the instability rolls (four times in one period for $\gamma = 1$). We observe that the instability bursts are characterized by a fast growth of the amplitude of the rolls followed by a relaxation exhibiting oscillations for large Taylor numbers ($Ta \geqslant 500$). These particular features are addressed in more detail in the following subsections.

We also observe that in any period, whatever the Taylor number, the flow velocity is practically zero at the times $t \approx 0.3$ and 0.8. These times correspond to the flow reversing its direction. Our measurements thus show experimental evidence that the transient or pulsed behaviour of the instability rolls is preserved at large amplitudes of modulation, i.e. at large Taylor numbers. Note that the temporal appearance and disappearance of the rolls is not clear when using only visualization, since with this

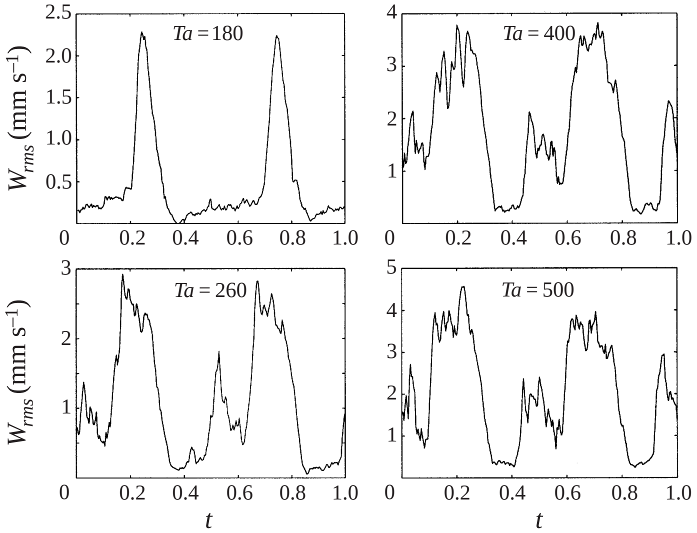

FIGURE 5. Examples of the behaviour of W_{rms} over one period for several Taylor numbers Ta and for $\gamma = 2$ and $Ro = 0$ ($\delta = 0.112$). The beginning of the period corresponds to cylinders at rest.

method rolls seem to exist permanently in the fluid when the forcing amplitude is large. However, we think that in our configuration, visualization is appropriate for the onset determination.

By comparing the axial profiles $w(z)$ at different times, we also observe that the flow is synchronized with the forcing, even at large Taylor numbers. In fact, the rolls organize themselves in order to alternate their vorticity from one half-period to the other. Sometimes however, perturbations to this alternation arise from the nucleation of a roll at the border due to the Ekman layer that develops in the same manner for a forward or backward movement of the cylinders.

Experiments for $\gamma = 1$ have been performed by either increasing or decreasing progressively the Taylor number. No significant difference has been observed in the behaviour of W_{rms} concerning the times of appearance and disappearance of the secondary flow and its amplitude values. We did not observe a significant difference for the instability threshold either. We believe that the absence of hysteresis is due to the temporal regions of flow restabilization in a period. In these regions, the perturbations are reduced to a residual level which is the same whether proceeding by small increments or decrements in the Taylor number.

5.1. *Amplitude dependence on the Taylor number*

Figure 6 presents the evolution with the Taylor number Ta of the maximal amplitude of $W_{rms}(t)$ for the mean rotation $Ro = 0$ and the modulation frequency $\gamma = 1$. We first observe a very slow growth of the amplitude followed by a square-root growth law (Graham & Domaradzki 1982). Note that the parameter range for the slow growth extends about 25% above the threshold. The same type of amplitude evolution with the Taylor number was also observed by Donnelly and coworkers in the case of a Taylor–Couette flow with temporal modulation (figure 3 of Donnelly, Reif & Suhl 1962 and figure 5 of Donnelly 1964). With regard to Donnelly's velocity behaviour, Hall (1983) has performed a nonlinear stability analysis at low frequencies, which indicates first a linear followed by a square-root growth of the amplitude.

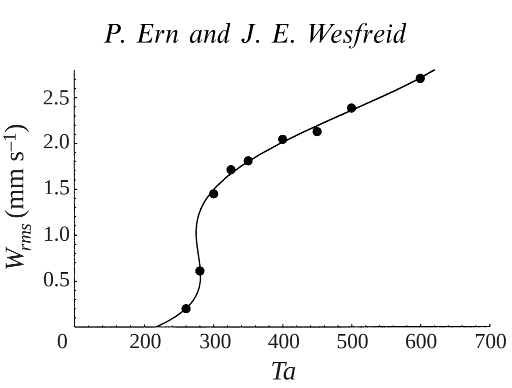

FIGURE 6. Evolution of the maximum value of W_{rms} over one period as a function of the Taylor number Ta for $Ro = 0$ and $\gamma = 1$ ($\delta = 0.112$).

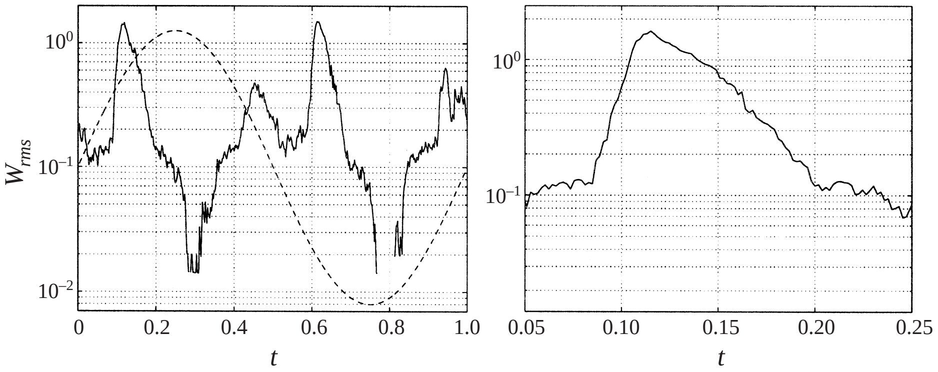

FIGURE 7. Examples of the evolution of W_{rms} over a period on a semi-logarithmic scale ($Ta = 325$, $Ro = 0$, $\gamma = 1$ and $\delta = 0.112$). The dashed line illustrates the shape of the forcing. An enlargement of the first instability peak is given on the right.

5.2. *Relaxation of the instability*

In most cases, the vortex structure develops in the flow with an exponential growth of the amplitude of the axial velocity component in a very short time, as shown in the semi-logarithmic plot of figure 7. Then, this velocity reaches its maximum value, studied in the previous section, and decays afterwards to a nearly zero value corresponding to the disappearance of the rolls. At large Taylor numbers, this relaxation presents oscillations in amplitude. A similar behaviour was observed by Kuhlmann *et al.* (1989) (see their figure 5) for a Taylor–Couette experiment with time-periodic inner cylinder rotation and fixed outer cylinder. Their results were obtained by direct numerical simulation and with a model based on a Galerkin approximation. As pointed out by these authors, temporal oscillations were also observed by Neitzel (1984) for the transient behaviour of Taylor vortices after cylinder rotation from a state of rest. Note however that the velocity decreases here independently of whether the forcing is increasing or decreasing (for the peaks at $\gamma = 1$, at the times $t \approx 0.15$ and $t \approx 0.65$ for instance), as illustrated in figure 7.

5.3. *Times of appearance and disappearance of secondary flow*

5.3.1. *Zero mean rotation flow*

We study the particular times of appearance and disappearance of secondary flow during one period and when $Ro = 0$. We have followed these times at a given

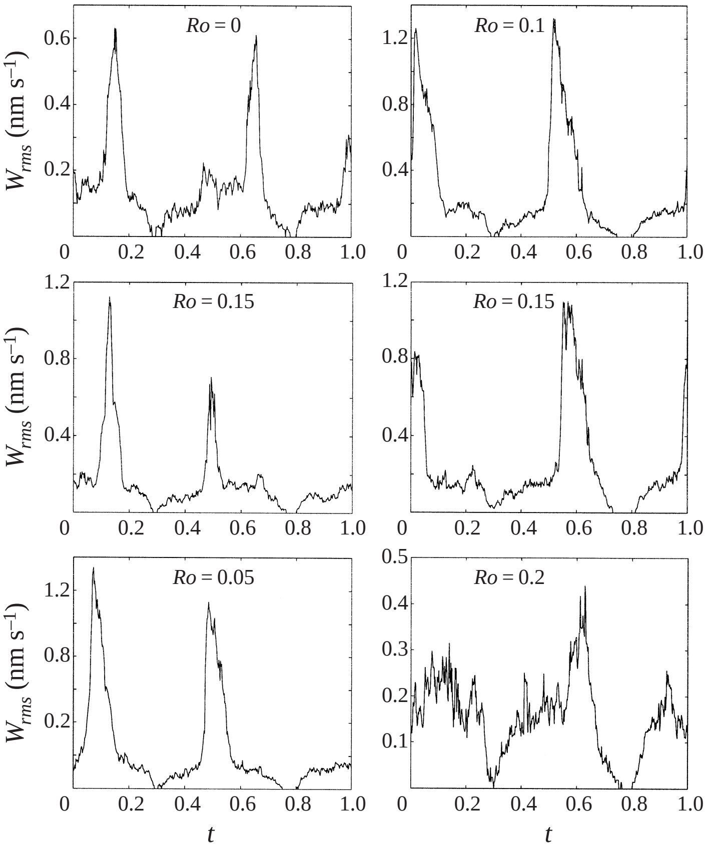

FIGURE 8. Examples of the behaviour of $W_{rms}(t)$ over one period for different rotation numbers and for $Ta = 280$ and $\gamma = 1$ ($\delta = 0.112$). The beginning of the period corresponds to cylinders at rest.

frequency when the Taylor number Ta increases. The results will be described in § 6.1 along with the numerical predictions. These times were extracted by considering as unstable temporal regions the ones where the velocity amplitude exceeds 0.15 mm s^{-1} in the $W_{rms}(t)$ evolution of figure 4.

5.3.2. *The effects of mean rotation*

We are interested in the modification of the behaviour of $W_{rms}(t)$ over one period when the rotation number Ro varies. Figure 8 presents $W_{rms}(t)$ over one period for $Ta = 280$, $\gamma = 1$ and different rotation numbers. For $Ro = 0.015$ and $Ta = 280$, we observe a stabilizing effect of the mean rotation during the second half-period with the disappearance of the W_{rms} peaks. Moreover, we observe that the rotation number affects the temporal regions of secondary flow. For instance, the first peak when $Ro = 0$ at $t \approx 0.1$ shifts towards $t \approx 0$ for $Ro \approx 0.1$ and then towards $t \approx 0.95$ for larger Ro. Note also the growth of a second peak that shifts from $t \approx 0.5$ (for $Ro = 0.015$) to $t \approx 0.65$ (for $Ro = 0.2$). For larger Ro, the peak tends to disappear and the flow is stable ($Ro \approx 0.3$). These results are recovered theoretically and numerically in § 6.

6. Theoretical analysis

The pulse-like behaviour of secondary flow observed experimentally in § 5 (see, for instance, figure 4) induced us to consider the linear stability analysis of the flow using a quasi-steady approach. This approach is valid as long as the rate of change of the flow is small compared to the growth rate of the perturbations. The sharp W_{rms} peaks observed experimentally correspond to a fast growth of the instability with respect to the flow period. Some previous theoretical studies dealt with the validity of the quasi-steady stability approach at low frequencies for time-dependent centrifugal flows. In particular, Seminara & Hall (1975) used a momentary stability criterion and calculated that the correction due to the slow time evolution of the perturbations is weak. Hall (1983) studied the nonlinear stability of slowly varying time-dependent viscous flows. He showed that, in most cases, quasi-steady analysis leads to the correct form of the solution except in the neighbourhood of the bifurcation point.

The quasi-steady stability of our system is analysed in the following two ways. In § 6.1, the linearized Navier–Stokes perturbation equations are recast as a first-order differential system with six unknowns, which is solved numerically at any given time with the corresponding velocity profile of the basic flow. In § 6.2, using the Navier–Stokes perturbation equations cast as a fourth-order differential system with two unknowns, we study analytically the dynamical similarity of our configuration to other systems in order to understand the instability development.

For convenience, we rescale the time by $t \rightarrow (2\pi/\omega)(t - \frac{1}{4})$ so that in the following $t = 0$ corresponds to cylinders at rest.

6.1. *Numerical calculations*

We denote the dimensional velocity by

$$\boldsymbol{U} = R_1 \; \Omega_o \; (0, V_B, 0) + (\tilde{u}, \tilde{v}, \tilde{w}),$$

and consider the velocity and pressure perturbations in the form

$$\left.\begin{aligned} (\tilde{u}, \tilde{v}, \tilde{w}) &= R_1 \; \Omega_o \; \mathrm{e}^{\mathrm{i}(\alpha t + m\theta + \lambda z)} \; (u, v, w), \\ \tilde{p} &= \frac{\rho \nu \Omega_o}{\delta} \; \mathrm{e}^{\mathrm{i}(\alpha t + m\theta + \lambda z)} \; \pi(x), \end{aligned}\right\} \tag{6.1}$$

with ρ being the density. Upon introducing the operators

$$\mathrm{D} = \frac{\partial}{\partial x}, \quad \mathrm{D}_* = \frac{\partial}{\partial x} + \xi(x) \quad \text{with} \quad \xi(x) = \frac{\delta}{1 + x\delta},$$

and $q = \lambda d$, $s = \alpha d^2/\nu$, $X = \mathrm{D}_* u(x) - \pi(x)$, the velocity perturbations are shown to be the solution of the following first-order differential system:

$$\left.\begin{aligned} \mathrm{D}_* u &= -\mathrm{i}m\xi v - \mathrm{i}qw, \\ \mathrm{D}_* v &= Y, \\ \mathrm{D}w &= Z, \\ \mathrm{D}X &= M(x)u + 2(\mathrm{i}m\xi^2 - \xi V_B Ta \;\, \delta^{-1/2})v, \\ \mathrm{D}Y &= (M(x) + m^2\xi^2)v - 2(\mathrm{i}m\xi^2 - \tfrac{1}{2}\mathrm{D}_* V_B Ta \;\, \delta^{-1/2})u - \mathrm{i}m\xi X + mq\xi w, \\ \mathrm{D}_* Z &= (M(x) + q^2)w - \mathrm{i}qX + mq\xi v, \end{aligned}\right\} \tag{6.2}$$

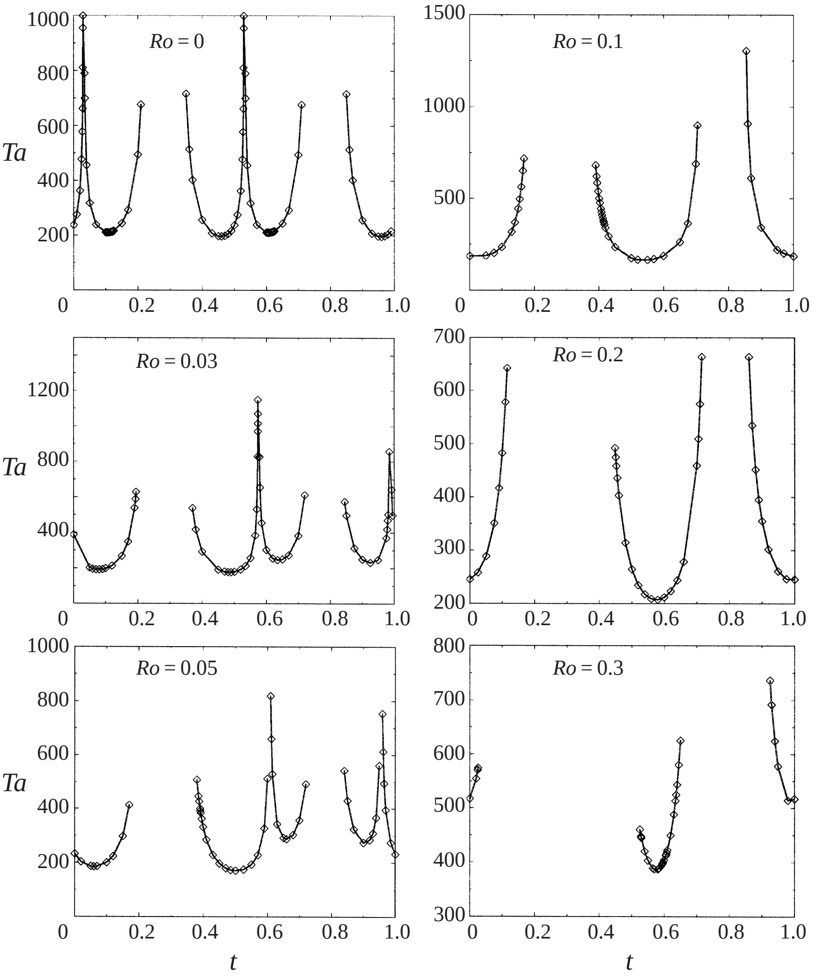

FIGURE 9. Examples of quasi-steady critical values of the Taylor number obtained by resolution of system (6.2) for axisymmetric neutral perturbations ($m = 0$, $s = 0$) for the frequency $\gamma = 1$ and several rotation numbers Ro ($\delta = 0.112$). The beginning of the period corresponds to cylinders at rest.

where $M(x) = q^2 + m^2\xi^2 + \mathrm{i}(s + m\xi V_B Ta\ \delta^{-1/2})$. The associated boundary conditions are

$$u = v = w = 0 \quad \text{for} \quad x = 0 \quad \text{and} \quad x = 1.$$

Using the general expression for the basic flow (2.4)–(2.6), the differential system (6.2) provides the linearized stability analysis in the finite-gap approximation. At fixed times, we solve numerically system (6.2) with a method similar to the one devised by Krueger, Gross & Di Prima (1966). We focus on neutral ($s = 0$) and axisymmetric ($m = 0$) perturbations. At any given time and at a given γ, we determine the critical parameters of instability Ta and q. The results obtained for $\gamma = 1$ and several rotations numbers, are presented in figure 9.

Figure 10 compares over one flow period (for $\gamma = 1$, $Ro = 0$) the instantaneous critical Taylor numbers Ta calculated from resolution of system (6.2) (solid line) to the experimental results (diamonds) obtained by extracting at different Taylor numbers

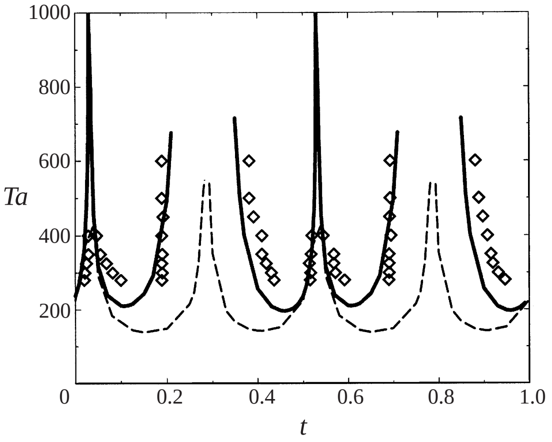

FIGURE 10. Times of appearance and disappearance of secondary flow, obtained experimentally (diamonds), numerically with a finite gap $\delta = 0.112$ (solid line) and using the small-gap approximation $\delta = 0$ (dashed line) for $\gamma = 1$ and $Ro = 0$. Time $t = 0$ corresponds to cylinders at rest.

the times of appearance and disappearance of secondary flow as measured in § 5.3. We observe a good agreement between experimental and numerical results with the finite-gap quasi-steady stability analysis. Note the correct prediction of the temporal stability regions around $t \approx 0.3$ and 0.8 and the very short regions for $t \approx 0.02$ and 0.52.

The dashed line in figure 10 corresponds to numerical quasi-steady calculations using the small-gap approximation ($\delta \rightarrow 0$), which leads to a lower value of the instability threshold Ta. For instance, for $\gamma = 1$ and $Ro = 0$, experimental visualization gives $Ta_c \approx 205$ while the minimal Ta value for finite-gap ($\delta = 0.112$) quasi-steady calculations is $Ta_c = 196$ and the minimal Ta value for small-gap quasi-steady calculations is $Ta_c = 139$. Note that the instability appears experimentally with a slight delay with respect to the numerical prediction. Since the instability observed experimentally corresponds to perturbations having a finite growth rate, it is natural that the experimental results concerning the appearance of the rolls lag behind the quasi-steady neutral stability curve. This behaviour is also in agreement with the results by Squire, Jankowski & Neitzel (1986) for the appearance (disappearance) of the vortex structure in a Taylor–Couette experiment during constant acceleration (deceleration) of the inner cylinder.

Table 1 presents, for several rotation numbers Ro, the times of appearance and disappearance of the vortex structure at frequency $\gamma = 1$ and Taylor number $Ta = 350$, obtained numerically and experimentally from § 5.3. Note the good agreement indicating that the mean rotation effect on the times of appearance and disappearance of secondary flow is also well recovered by the quasi-steady finite-gap analysis.

For $\gamma = 1$, figure 11 presents as a function of the rotation number the minimal values in one period of the Taylor number, obtained numerically (filled triangles), and the experimental results for the onset of instability (circles), yielding quite good agreement.

These results indicate that the finite-gap quasi-steady analysis may be successfully applied in this time-dependent flow configuration up to intermediate frequencies ($\gamma \lesssim 1$). For higher frequencies, this agreement worsens and breaks down for $\gamma \approx 2$, as shown in Ern (1997). Note that there is also a good agreement with small-gap Floquet

Ro		Times							
		(d)	(a)	(d)	(a)	(d)	(a)	(d)	(a)
0	num.	0.02	0.05	0.19	0.38	0.52	0.55	0.69	0.88
	exp.	0.02	0.06	0.19	0.40	0.52	0.56	0.69	0.90
0.05	num.	0.16	0.40	0.59	0.63	0.70	0.87	0.94	0.98
	exp.	0.16	0.40	0.60	0.65	0.71	0.90		
0.10	num.	0.14	0.42	0.67	0.90				
	exp.	0.13	0.44	0.66	0.91				
0.20	num.	0.08	0.47	0.67	0.90				
	exp.	0.10	0.50	0.68	0.94				

TABLE 1. For four rotation numbers *Ro*, times of appearance (a) and disappearance (d) of secondary flow for $Ta = 350$ and $\gamma = 1$ ($\delta = 0.112$), obtained numerically (num.) from § 6.1 and experimentally (exp.) from § 5.3. Time $t = 0$ corresponds to cylinders at rest.

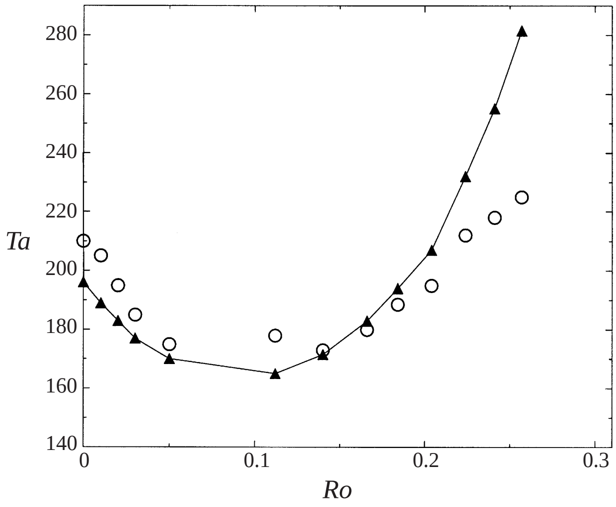

FIGURE 11. Comparison of the stability results for $\gamma = 1$ as a function of the rotation number *Ro*. The circles (○) correspond to the experimental results by visualization and the filled triangles (▲) to the minimum value over a period of the Taylor numbers obtained numerically ($\delta = 0.112$) with the quasi-steady calculations of § 6.1.

calculations performed when $Ro = 0$, yielding $Ta_c = 197$ for $\gamma = 1$ (C. Normand 1998, personal communication).

Finally, we illustrate in figure 12 the evolution of the quasi-steady Taylor number *Ta* associated with the times $t = 0.10$, $t = 0.25$ ($\sin t = 0$) and $t = 0.50$ ($\cos t = 0$) in a continuous range of gap width δ ($\gamma = 1$, $Ro = 0$). Note the rapid stabilization of the flow with increasing gap width at $t = 0.25$.

6.2. *Some analytical considerations*

For convenience, we adopt now the following non-dimensional variables (u, v, w) such that $\tilde{u} = -(\nu/2d)u$, $\tilde{v} = \frac{1}{2}R_1\Omega_o v$ and $\tilde{w} = -(\nu/2d)w$ where $(\tilde{u}, \tilde{v}, \tilde{w})$ are still the perturbations to the basic flow. The space variable z is made non-dimensional with the gap width d. For axisymmetric flows, the Navier–Stokes equations for $(\tilde{u}, \tilde{v}, \tilde{w})$ can be recast after linearization as a two-equation system of order 4 for the

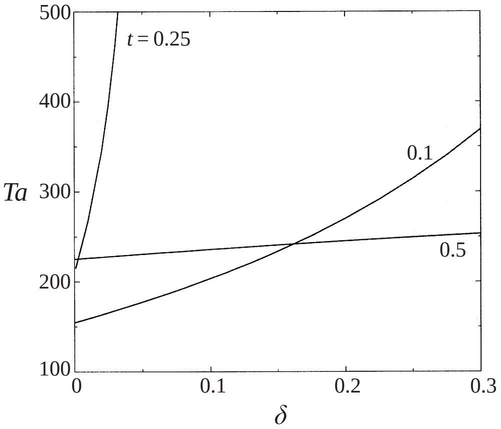

FIGURE 12. Examples of the evolution with the gap size δ of the quasi-steady Taylor number Ta associated with the times $t = 0.10$, $t = 0.25$ and $t = 0.50$ ($\gamma = 1$, $Ro = 0$).

radial and azimuthal perturbation velocities u and v (see, for instance, Hall 1975 or Chandrasekhar 1981). The perturbation velocities then satisfy

$$\left.\begin{aligned} \left(\mathrm{DD}_* - q^2 - \frac{\partial}{\partial \tau}\right)(\mathrm{DD}_* - q^2)u = 2q^2 Ta^2 \frac{V_B}{1+\delta x}v, \\ \left(\mathrm{DD}_* - q^2 - \frac{\partial}{\partial \tau}\right)v = (\mathrm{D}_* V_B)u, \end{aligned}\right\} \tag{6.3}$$

with boundary conditions

$$u = v = \frac{\partial u}{\partial x} = 0 \quad \text{for} \quad x = 0 \quad \text{and} \quad x = 1. \tag{6.4}$$

6.2.1. *Low-frequency analysis*

In this subsection, we recover the stability or instability of the azimuthal basic flow at some particular times through a straightforward analytical approach. We focus on the case of low frequencies $\sigma = 2\gamma^2 \ll 1$ and perform a quasi-steady linear stability analysis assuming $\partial/\partial\tau \to 0$. In this framework, the time appears only as a parameter through the basic flow V_B. For simplicity, we analyse the neutral stability of axisymmetric perturbations. Finally, in order to apply classical results for steady centrifugal flows, we consider the differential operators on the left-hand side of the system in the small-gap approximation ($\delta \to 0$). We keep however the right-hand term of the system which includes the basic flow in its finite-gap expression ($\delta^2 \ll 1$). The good agreement of the results of this subsection with those of the previous one, performed with a complete finite-gap approach, supports this latter simplification, showing that the main finite-gap effect is related to the basic flow and that curvature effects in the diffusion term may be neglected in our system. In this framework, system (6.3) reduces to

$$\left.\begin{aligned} (\mathrm{D}^2 - q^2)^2 u &= 2q^2 Ta^2 \frac{V_B}{1+\delta x}v, \\ (\mathrm{D}^2 - q^2)v &= (\mathrm{D}_* V_B)u, \end{aligned}\right\} \tag{6.5}$$

with boundary conditions (6.4). For low frequencies $\sigma \ll 1$ and since $\delta < \gamma$, the basic flow is given by (2.8) at the order $\gamma^2\delta$

$$\left.\begin{aligned} V_B &= (\hat{Ro} + \cos\sigma\tau)(1+\delta x) + \gamma^2 x(1-x)(1+\tfrac{1}{2}\delta)\sin\sigma\tau + o(\gamma^2\delta), \\ \mathrm{D}_* V_B &= 2\delta(\hat{Ro} + \cos\sigma\tau) + \gamma^2\left((1-2x)(1+\tfrac{1}{2}\delta) + \delta x(1-x)\right)\sin\sigma\tau + o(\gamma^2\delta), \end{aligned}\right\} \tag{6.6}$$

as presented in § 2. We now review the stability of the perturbation system (6.5) along with basic flow expressions (6.6) as a function of the rotation number $Ro = \hat{Ro}\ \delta$.

Let us first consider the case where the rotation rate $\hat{Ro}$ is predominant in (6.6), that is $\hat{Ro} \gg 1$, and the equations hence read at the first order

$$\left.\begin{aligned} (\mathrm{D}^2 - q^2)^2 u &= 2q^2 Ta^2 \hat{Ro} v \equiv q^2 A v, \\ (\mathrm{D}^2 - q^2) v &= 2\hat{Ro}\delta u \equiv -Bu. \end{aligned}\right\} \tag{6.7}$$

This system takes the form of Rayleigh–Bénard convection equations for a fluid of Prandtl number $P_r = 1$ (Chandrasekhar 1981) with parameters $A = 2\ Ta^2\hat{Ro}$ and $B = -2\ \hat{Ro}\ \delta$. As the equivalent Rayleigh number $Ra = A \times B$ is negative, the system is stable. For sufficiently large Ro, the flow is thus stable, as observed experimentally.

We consider now the preceeding order of magnitude for the rotation number which is given in (6.6) when $\hat{Ro}\ \delta \sim \gamma^2$ and when neglecting higher-order terms, like $\gamma^2\delta$. The velocity then reads $V_B = (1+\delta x)(\hat{Ro} + \cos\sigma\tau)$ and its derivative $\mathrm{D}_* V_B = 2\delta(\hat{Ro} + \cos\sigma\tau) + \gamma^2(1-2x)\sin\sigma\tau$. Rescaling u and v, the stability equation system (6.5) appears then in the adjoint form to the Taylor–Couette system (Chandrasekhar 1981)

$$\left.\begin{aligned} (\mathrm{D}^2 - q^2)^2 u &= -q^2 \hat{T} v, \\ (\mathrm{D}^2 - q^2) v &= (1+\alpha x) u, \end{aligned}\right\} \tag{6.8}$$

with

$$\alpha = \frac{-2\gamma^2 \sin\sigma\tau}{F}, \quad \hat{T} = -2\ Ta^2\ (\hat{Ro} + \cos\sigma\tau)\ F \quad \text{and} \quad F = 2(\hat{Ro} + \cos\sigma\tau)\delta + \gamma^2\sin\sigma\tau.$$

Quasi-steady instability is therefore possible for times such that $\hat{T} > 0$. For the time intervals for which (6.8) is valid, we have $\alpha \leqslant -2$ and we can thus apply the asymptotic relation given by Chandrasekhar (1981) for strongly counter-rotating Taylor–Couette flow $\hat{T}(\alpha) \approx 1180\ \alpha^4$. We get

$$Ta \approx \left(\frac{-9440\gamma^8}{G}\right)^{1/2} \quad \text{with} \quad G = \frac{(\hat{Ro} + \cos\sigma\tau)F^5}{\sin^4\sigma\tau}. \tag{6.9}$$

Figure 13 shows a plot of the negative values of G over one period for different rotation numbers. This evolution of G shows that when $Ro = 0$, two symmetrical temporal regions of secondary flow exist that evolve differently as the rotation number is increased. In one temporal region ($t \approx 0.55$), the flow undergoes rapid stabilization whereas in the other ($t \approx 0.05$), it is first slightly destabilized and ultimately stabilized with the mean rotation.

It is particularly interesting to consider the Taylor number value Ta_{TC} obtained from (6.9) for the critical time t_{TC} such that $G < 0$ and G is maximal in absolute value. This time corresponds to the moment at which this type of instability

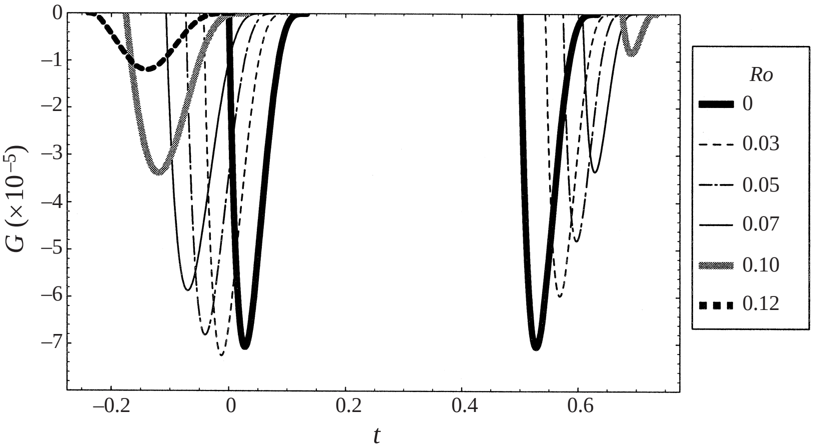

FIGURE 13. Evolution over one period of the regions $G < 0$ as a function of the rotation number Ro for $\gamma = 0.5$ ($\delta = 0.112$). G is defined by equation (6.9).

may be first observed in the system. The evolution with the rotation number of the Taylor number Ta_{TC} associated with the time t_{TC} for both temporal regions is presented in figure 14. These results are presented for $\gamma = 1$ in order to compare them with the results of the previous sections. We observe a good agreement between these results (solid line) and those (circles) obtained by solving the complete system in § 6.1 and taking the local minimal value of the instantaneous Taylor number for the times concerned. Instability in the system can thus be attributed in the temporal regions of figure 10 around $t \approx 0.1$ and 0.6 to a counter-rotating Taylor–Couette type behaviour. We have checked that the behaviour of t_{TC} and Ta_{TC} with Ro is identical at lower frequencies ($\gamma = 0.35$ and $\gamma = 0.5$) (Ern 1997). Moreover, whatever the frequency γ, stabilization of the second temporal region is observed from the curve $Ta_{TC} = f(Ro)$ as $Ro \to \delta = 0.112$ or $\Omega_m/\Omega_o \to 1$ (dashed curve in figure 14). The lowest curve in figure 14 corresponds to the small-gap approximation results, showing again a lower evaluation of the threshold. For instance, when $Ro = 0$, we have $\alpha \approx -2.4$ when considering $\delta = 0.112$, yielding $Ta_{TC} = 206$ for $\gamma = 1$, whereas when the small-gap approximation is used, we get $\alpha = -2$ and $Ta_{TC} = 136$.

Our results also show that the time t_{TC} evolves towards an asymptotic value $t^{\infty}_{TC}(\gamma)$ at large rotation numbers (for $\gamma = 1$, $t^{\infty}_{TC} \approx 0.95$). In fact, at a given frequency γ, when the condition $Ro > \cos t^{\infty}_{TC}$ is achieved, the sign of F only determines the existence of a $Ta > 0$. Hence, the asymptotic time corresponds to the minimum of F and reads $t^{\infty}_{TC}(\gamma) = \arctan(\gamma^2/(2\delta))$. The value of the rotation number Ro for which $F(t) > 0 \ \forall \ t$, called Ro^S_{lim}, corresponds to a limit rotation number above which no instability is observed, according to this stability analysis for the relevant time period. This limit rotation number, given by $F(t^{\infty}_{TC}, Ro^S_{lim}) = 0$, reads

$$Ro^S_{lim} = \tfrac{1}{2}\left(\gamma^4 + 4\delta^2\right)^{1/2}. \tag{6.10}$$

Note that this estimation of the limit rotation number is very close to the prediction of the Rayleigh discriminant, both estimations being proportional to γ^2, when $4\delta^2 \ll \gamma^4$ (see § 4.2). Note also that with the expression for t^{∞}_{TC}, it is straightforward to derive an

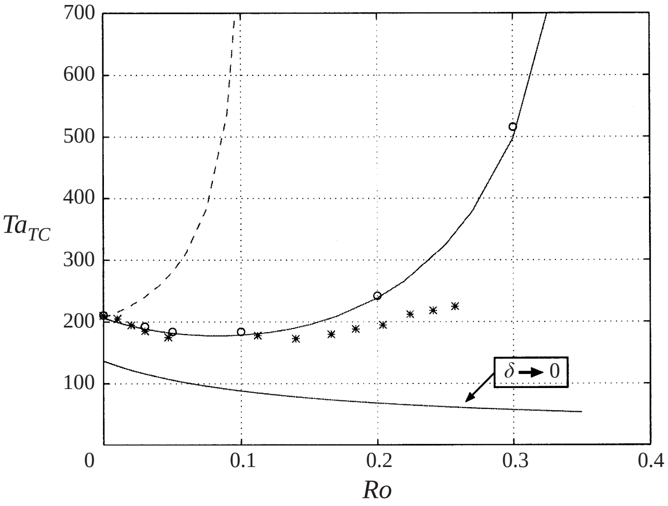

FIGURE 14. Evolution of Ta_{TC} corresponding to the minimum of expression (6.9) for both half-periods (solid and dashed lines) as a function of the rotation number Ro for $\gamma = 1$ ($\delta = 0.112$). The circles are the results obtained by solving the complete system of § 6.1 and taking the local minimum value of the instantaneous Taylor number for the temporal region concerned. (The crosses denote the experimental results of figure 11.) Results obtained using the small-gap approximation $\delta \rightarrow 0$ are also presented, giving a lower value of the threshold.

asymptotic analytic expression for the Taylor number Ta_{TC} at large rotation numbers, as shown in Ern (1997).

Another interesting case in the stability equations (6.5) appears when $\hat{R}o \leqslant 1$ and for the times t_0 such that $\hat{R}o + \cos t_0$ is sufficiently small to be negligible in the expressions (6.6) for V_B and $D_* V_B$, as well as the terms of order $\gamma^2\delta$. Note that, for instance for $Ro = 0$, these time values are $t_0 = 0.5$ and 1 which belong to the second and fourth unstable temporal regions of figure 10. We introduce $\hat{T}a^2 = Ta^2\gamma^4 = O(1)$ so that system (6.5) now reads

$$\left.\begin{aligned} (\mathrm{D}^2 - q^2)^2\, u &= 2q^2 \hat{T}a^2 x(1-x)\sin t_0\, v \equiv -q^2 \mathrm{D}x(1-x)v, \\ (\mathrm{D}^2 - q^2)v &= (1-2x)\sin t_0\, u \equiv (1-2x)u. \end{aligned}\right\} \qquad (6.11)$$

After rescaling u and v, these equations correspond to Dean's problem (Chandrasekhar 1981), as shown on the right, thus giving the following dependence of the critical Taylor number Ta_D on the rotation number: $Ta_D \approx 215\,\gamma^{-2}\,(1-\hat{R}o^2)^{-1/2}$. For $\hat{R}o = 0$ and $\gamma = 1$, we get $Ta_D = 215$ and for $\gamma = 0.5$, $Ta_D = 870$. The dependence of Ta_D on the rotation number shows a strong stabilizing effect of the mean rotation on this instability of Dean type. This instability may be observed for a time that evolves, as the rotation number increases, from $t_0 = 0.5$ to 0.75 and from $t_0 = 1$ to 0.75.

Finally, in the particular case when $\sin t = 0$ and therefore $\cos t = \pm 1$, the stability equation system (6.5) reduces to

$$\left.\begin{aligned} (\mathrm{D}^2 - q^2)^2 u &= 2q^2 Ta^2(\hat{R}o \pm 1)v, \\ (\mathrm{D}^2 - q^2)v &= 2\delta(\hat{R}o \pm 1)u, \end{aligned}\right\} \qquad (6.12)$$

which is, as for equations (6.7), a stable Rayleigh–Bénard convection system. Hence, whatever the rotation number Ro, the system is stable at the times such that $\sin t = 0$,

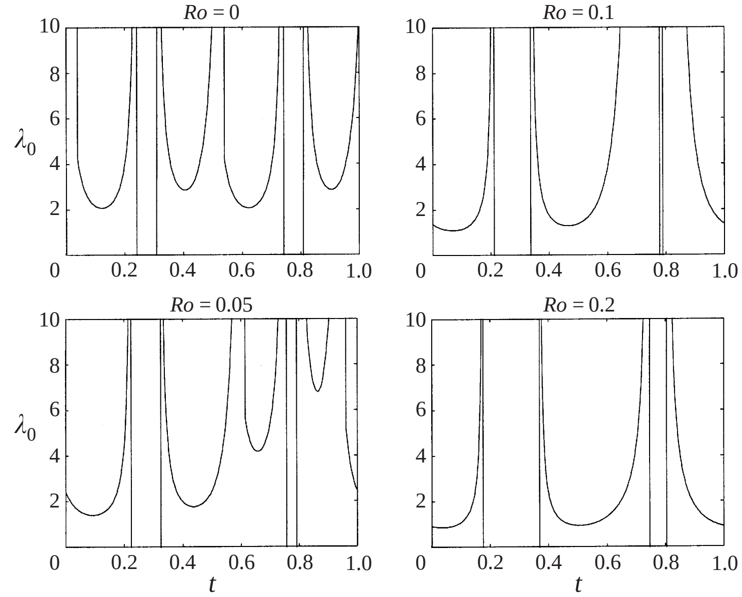

FIGURE 15. Examples of the evolution over a period of the Taylor number coefficient λ_0 for several rotation numbers *Ro* and for $\gamma = 1$ ($\delta = 0.112$), as obtained using the criterion of Hall (1982). Vertical lines represent asymptotes. The beginning of the period corresponds to cylinders at rest. Note the similarity with figure 9.

as is also observed experimentally in figure 8 where the axial velocity value W_{rms} is zero at that times. Note that this effect can only be recovered using a finite-gap approach.

6.2.2. *Quasi-steady approach using the criterion of Hall (1982)*

At higher frequencies, following the approach of Horseman *et al.* (1996), it may be interesting to apply an analytical result of Hall (1982) concerning the asymptotic linear stability analysis of centrifugal instabilities at large wavenumbers. At higher frequencies, these authors considered that the growth rate of the perturbations is still larger than the time scale associated with the modulation and also that the characteristic size of the vortex structures is given by the Stokes layer thickness which is small with respect to the gap, thus corresponding to large wavenumbers. However, as observed in the previous sections, we have to consider finite-gap effects, which amounts only to considering the finite-gap expression for the Rayleigh discriminant (Ern 1997). We denote $2\ Ta^2 \approx \lambda_0 \epsilon^{-4}$ at first order, with $\epsilon^{-1} = q \gg 1$ the wavelength non-dimensionalized with the gap d and λ_0 being a constant. For acceptable solutions of the stability equations, we need $\Phi < 0$ and $\lambda_0 > -\Phi_{min}^{-1}$ where Φ_{min} is the minimum value of the finite-gap Rayleigh discriminant Φ which reads

$$\Phi = \frac{V_B}{1 + \delta x}\,(\mathrm{D}_* V_B).$$

For a given time t, we determine the position of the minimum value of Φ for the associated velocity profile and then the Taylor number coefficient λ_0. Figure 15 presents the λ_0 values over a period for different rotation numbers and for $\gamma = 1$. The results compare satisfactorily with figure 9 for the prediction of the times when secondary flow exists, even for this intermediate frequency. However, we do not know the wavenumbers so that the Ta values associated with the λ_0 cannot be determined.

7. Conclusions

In this paper, we have studied the stability of the flow induced by the time-periodic co-rotation of two concentric cylinders at the angular velocity $\Omega(t) = \Omega_m + \Omega_o \cos \omega t$ by visualization and ultrasound Doppler velocimetry. A first contribution of our work concerns the competing effects of the centrifugal and the Coriolis forces on the flow stability, which is analysed at a given frequency by progressively increasing the rotation number $Ro = \delta\Omega_m/\Omega_o$. Over a large range of this parameter and for several forcing frequencies, we have shown by visualization that the flow is first destabilized as compared to the purely centrifugal case and then restabilized progressively until complete restabilization. This ultimate restabilization can be analysed with the Rayleigh criterion and corresponds to a Taylor–Proudman effect. The most original contribution of this work is the analysis of the time-dependent behaviour of the secondary flow. Velocity field measurements in the rotating frame of the cylinders were performed by an ultrasound Doppler apparatus. The global axial velocity value $W_{rms}(t)$ was used to analyse the evolution of the secondary flow over a time period. We have observed that vortex structures appear and disappear several times during one period, even at large Taylor numbers. The effect of the mean rotation on the time evolution of $W_{rms}(t)$ has been also addressed.

Our experimental observations of the transient flow behaviour and earlier theoretical studies (Seminara & Hall 1975; Hall 1983) on the validity of the quasi-steady stability analysis motivated us to analyse the linear stability of the basic flow with this approach, which allows us to obtain the times of appearance and disappearance of the secondary flow. We established an analytical solution of the basic flow, valid for a finite-gap and determined numerically the linear instability threshold for different times. The quasi-steady linear stability analysis was compared to experimental velocity measurements. The good agreement obtained in this configuration is valid up to intermediate frequencies ($\gamma \lesssim 1$). This agreement worsens at higher frequencies ($\gamma > 1$). The results obtained experimentally and with the quasi-steady approach are the following: flow destabilization and restabilization when the mean rotation is increased; prediction of the particular times of appearance and disappearance of the secondary flow for several Taylor numbers; and the effect of the mean rotation on these times. We have also shown by analytical considerations that our system is dynamically similar (same stability equations) at some particular times to well-documented systems (like counter-rotating Taylor–Couette, Dean or Rayleigh–Bénard flows). This result provides an interpretation of the flow stability and instability at particular times, as observed experimentally and numerically. We also point out that the quasi-steady analysis has to take into account the finite gap, as a lower evaluation of the instability threshold is obtained in our case when using the small-gap approximation ($\delta \to 0$).

In summary, we have shown that instability may be substantially modified by solid-body rotation or time periodicity and that a simple theoretical analysis may give valuable information on the flow behaviour. An interesting prospect for future work is to use the technique of phase-averaging, in order to determine, at a given phase-time, the unsteady characteristics of the root-mean-square value $W_{rms}(t)$ over different cycles. Phase-averaged values of the axial velocity component $w(z_i, t)$ may also be retrieved for spatial locations z_i to characterize the spatio–temporal behaviour of the vortex structure.

The authors are indebted to A. Ern for useful comments and for developing the numerical code used in § 6. Discussions with M. Lücke, D. Tritton, C. Normand, A. Stegner and A. Aouidef are gratefully acknowledged. We also would like to thank M. Willemetz for technical advice concerning the ultrasound Doppler velocimetry.

REFERENCES

AHLERS, G., CANNELL, D., DOMINGUEZ-LERMA, M. & HEINRICHS, R. 1986 Wavenumber selection and Eckhaus instability in Couette–Taylor flow. *Physica* D **23**, 202–219.

AHLERS, G., HOHENBERG, P. & LÜCKE, M. 1985 Thermal convection under external modulation of the driving force. I: The Lorenz model- II: Experiments. *Phys. Rev.* A **32**, 3493–3534.

ALFREDSSON, P. & PERSSON, H. 1989 Instabilities in channel flow with system rotation. *J. Fluid Mech.* **202**, 543–557.

ANDERECK, D., LIU, S. & SWINNEY, H. 1986 Flow regimes in a circular Couette system with independently rotating cylinders. *J. Fluid Mech.* **164**, 155–183.

AOUIDEF, A., NORMAND, C., STEGNER, A. & WESFREID, J.-E. 1994 Centrifugal instability of pulsed flow. *Phys. Fluids* **6**, 3665–3676.

AOUIDEF, A., WESFREID, J.-E. & MUTABAZI, I. 1992 Coriolis effects on Görtler vortices in the boundary layer flow on concave wall. *AIAA J.* **30**, 2779–2782.

BARENGHI, C. & JONES, C. 1989 Modulated Taylor–Couette flow. *J. Fluid Mech.* **208**, 127–160.

BIDOKHTI, A. & TRITTON, D. 1992 The structure of a turbulent free shear layer in a rotating fluid. *J. Fluid Mech.* **241**, 469–502.

CAMBON, C., BENOIT, J. P., SHAO, L. & JACQUIN, L. 1994 Stability analysis and large-eddy simulation of rotating turbulence with organized eddies. *J. Fluid Mech.* **278**, 175–200.

CARMI, S. & TUSTANIWSKYJ, J. 1981 Stability of modulated finite-gap cylindrical Couette flow: linear theory. *J. Fluid Mech.* **108**, 19–42.

CHANDRASEKHAR, S. 1981 *Hydrodynamic and Hydromagnetic Instability*. Dover.

COOPER, E., JANKOWSKI, D., NEITZEL, G. & SQUIRE, T. 1985 Experiments on the onset of instability in unsteady circular Couette flow. *J. Fluid Mech.* **161**, 97–113.

DAVIS, S. 1976 The stability of time-periodic flows. *Ann. Rev. Fluid Mech.* **8**, 57–74.

DONNELLY, R. 1964 Experiments on the stability of viscous flow between rotating cylinders. III. Enhancement of stability by modulation. *Proc. R. Soc. Lond.* A **281**, 130–139.

DONNELLY, R., REIF, F. & SUHL, H. 1962 Enhancement of hydrodynamic stability by modulation. *Phys. Rev. Lett.* **9**, 363–365.

EAGLES, P. 1977 On the stability of slowly varying flow between concentric cylinders. *Proc. R. Soc. Lond.* A **355**, 209–224.

ERN, P. 1997 Instabilités d'écoulements périodiques en temps avec effets de courbure et de rotation. Thèse de Doctorat, Université Paris VI, France.

ERN, P. 1998 A study on time-periodic finite-gap Taylor–Couette flows. *C. R. Acad. Sci. Paris* IIb **326**, 727–732.

GAUTHIER, G., GONDRET, P. & RABAUD, M. 1998 Motions of anisotropic particles: application to visualization of three-dimensional flows. *Phys. Fluids* **10**, 2147–2154.

GRAHAM, R. & DOMARADZKI, J. 1982 Local amplitude equation of Taylor vortices and its boundary condition. *Phys. Rev.* A **26** (3), 1572–1579.

HALL, P. 1975 The stability of unsteady cylinder flows. *J. Fluid Mech.* **67**, 29–63.

HALL, P. 1982 Taylor–Görtler vortices in fully developed or boundary layer flows: linear theory. *J. Fluid Mech.* **124**, 475–494.

HALL, P. 1983 On the nonlinear stability of slowly varying time-dependent viscous flows. *J. Fluid Mech.* **126**, 357–368.

HEINRICHS, R., CANNELL, W., AHLERS, G. & JEFFERSON, M. 1988 Experimental test of the perturbation expansion for the Taylor instability at various wavenumbers. *Phys. Fluids* **31**, 250–255.

Horseman, N., Bassom, A. & Blennerhassett, P. 1996 Strongly nonlinear vortices in the Stokes layer on an oscillating cylinder. *Proc. R. Soc. Lond.* A **452**, 1087–1111.

Kloosterziel, R. & Heijst, G. van 1991 An experimental study of unstable barotropic vortices. *J. Fluid Mech.* **223**, 1–24.

Krueger, E., Gross, A. & Di Prima, R. 1966 On the relative importance of Taylor-vortex and non-axisymmetric modes in flow between rotating cylinders. *J. Fluid Mech.* **24**, 521–538.

Kuhlmann, H., Roth, D. & Lücke, M. 1989 Taylor-vortex flow under harmonic modulation of the driving force. *Phys. Rev.* A **39**, 745–762.

Leblanc, S. & Cambon, C. 1997 On the three-dimensional instabilities of plane flows subjected to Coriolis force. *Phys. Fluids* **9**, 1307–1316.

Matsson, O. & Alfredsson, P. 1990 Curvature- and rotation-induced instabilities in channel flow. *J. Fluid Mech.* **210**, 537–563.

Matsson, O. & Alfredsson, P. 1994 The effect of spanwise system rotation on Dean vortices. *J. Fluid Mech.* **274**, 243–265.

Mutabazi, I., Normand, C. & Wesfreid, J.-E. 1992 Gap size effects on centrifugally and rotationally driven instabilities. *Phys. Fluids* A **4**, 1199–1205.

Mutabazi, I. & Wesfreid, J.-E. 1993 Coriolis force and centrifugal force induced flow instabilities. In *Mathematics and its Applications: Instabilities and Nonequilibrium Structures*, vol. 4 (ed. E. Tirapegui & W. Zeller), pp. 301–316. Kluwer.

Neitzel, G. 1984 Numerical computation of time-dependent Taylor-vortex flows in finite-length geometries. *J. Fluid Mech.* **141**, 51–66.

Ning, L., Tveitereid, M., Ahlers, G. & Cannel, D. 1991 Taylor–Couette flow subjected to external rotation. *Phys. Rev.* A **44**, 2505–2513.

Papageorgiou, D. 1987 Stability of the unsteady viscous flow in a curved pipe. *J. Fluid Mech.* **182**, 209–233.

Pexieder, A. 1996 Effects of system rotation on the centrifugal instability of the boundary layer on a curved wall: an experimental study. PhD thesis no. 1507, Ecole Polytechnique Fédérale de Lausanne, Switzerland.

Rosenblat, S. 1968 Centrifugal instability of time-dependent flows. Part 1. Inviscid, periodic flows. *J. Fluid Mech.* **33**, 321–336.

Schmitt, S. & Lücke, M. 1991 Amplitude equation for modulated Rayleigh–Bénard convection. *Phys. Rev.* A **44**, 4986–5002.

Seminara, G. & Hall, P. 1975 Linear stability of slowly varying unsteady flows in a curved channel. *Proc. R. Soc. Lond.* A **346**, 279–303.

Seminara, G. & Hall, P. 1976 Centrifugal instability of a Stokes layer: linear theory. *Proc. R. Soc. Lond.* A **350**, 299–316.

Seminara, G. & Hall, P. 1977 The centrifugal instability of a Stokes layer: nonlinear theory. *Proc. R. Soc. Lond.* A **354**, 119–126.

Squire, T., Jankowski, D. & Neitzel, G. 1986 Experiments with deceleration from a Taylor-vortex flow. *Phys. Fluids* **29**, 2742–2743.

Takeda, Y. 1991 Development of an ultrasound velocity profile monitor. *Nucl. Engng Des.* **126**, 277–284.

Takeda, Y., Fischer, W. & Sakakibara, J. 1993*a* Measurement of energy spectral density of a flow in a rotating Couette system. *Phys. Rev. Lett.* **70**, 3569–3571.

Takeda, Y., Fischer, W., Sakakibara, J. & Ohmura, K. 1993*b* Experimental observation of the quasiperiodic modes in a rotating Couette system. *Phys. Rev.* E **47**, 4130–4134.

Tennakoon, S., Andereck, D., Aouidef, A. & Normand, C. 1997 Pulsed flow between concentric rotating cylinders. *Eur. J. Mech.* B **16**, 227–248.

Tritton, D. & Davies, P. 1985 Instabilities in geophysical fluid dynamics. In *Topics in Applied Physics, vol. 45: Hydrodynamic Instabilities and the Transition to Turbulence* (ed. H. Swinney & J. Gollub), pp. 229–270. Springer.

Tustaniwskyj, J. & Carmi, S. 1980 Nonlinear stability of modulated finite-gap Taylor flow. *Phys. Fluids* **23**, 1732–1739.

Walsh, T. 1988 The influence of external modulation on the stability of azimuthal Taylor–Couette flow: an experimental investigation. PhD thesis, University of Oregon, USA.

Wiener, R., Hammer, P., Swanson, C. & Donnelly, R. 1990 Stability of Taylor–Couette flow subject to an external Coriolis force. *Phys. Rev. Lett.* **64**, 1115–1118.

Willemetz, J. 1990 Etude quantitative de l'hémodynamique de vaisseaux profonds par Echographie Doppler Ultrasonore. Thèse no. 893, Ecole Polytechnique Fédérale de Lausanne, Switzerland.

Zebib, A. & Bottaro, A. 1993 Görtler vortices with system rotation: linear theory. *Phys. Fluids* A **5**, 1206–1210.